

# An upgraded interpolator of the radial basis function network for spectral calculation based on empirical stellar spectral library

Lian-Tao Cheng<sup>1,2,3,4</sup> and Feng-Hui Zhang<sup>1,2,3</sup>

<sup>1</sup> Yunnan Observatories, Chinese Academy of Sciences, Kunming 650216, China; [clt252206@sina.cn](mailto:clt252206@sina.cn),  
[zhangfh@ynao.ac.cn](mailto:zhangfh@ynao.ac.cn)

<sup>2</sup> Center for Astronomical Mega-Science, Chinese Academy of Sciences, Beijing 100012, China

<sup>3</sup> Key Laboratory for the Structure and Evolution of Celestial Objects, Chinese Academy of Sciences, Kunming 650216, China

<sup>4</sup> University of Chinese Academy of Sciences, Beijing 100049, China

Received 2020 March 17; accepted 2020 April 3

**Abstract** Stellar population synthesis is an important method in galaxy and star-cluster studies. In stellar population synthesis models, a stellar spectral library is necessary for the integrated spectra of the stellar population. Usually, the stellar spectral library is utilized for the transformation between the stellar atmospheric parameters and stellar spectrum. The empirical stellar spectral library has distinct advantages over the theoretical library. However, for the empirical spectral library, the distribution of stars is irregular in the stellar atmospheric parameter space, which makes the traditional interpolator difficult to get accurate results. In this work, we will provide an improved radial basis function interpolator which is implemented to obtain the interpolated stellar spectra based on the empirical stellar spectral library. For this interpolator, we use the relation between the standard variance  $\sigma$  in the Gaussian radial basis function and the density distribution of stars in the stellar atmospheric parameter space to give the prior constraint on this  $\sigma$ . Moreover, we also consider the anisotropic radius basis function by the advantage of the local dispersion of stars in the stellar atmospheric parameter space. Furthermore, we use the empirical stellar spectral library MILES to test this interpolator. On the whole, the interpolator has a good performance except for the edge of the low-temperature region. At last, we compare this interpolator with the work in Cheng et al., and the interpolation result shows an obvious improvement. Users can apply this interpolator to retrieve the interpolated spectra based on the stellar spectral library quickly and easily.

**Key words:** stars: fundamental parameters—stars: atmospheres—(Galaxy:) globular clusters: general—methods: numerical

## 1 INTRODUCTION

A stellar population synthesis model is important in astronomical research. Most of the observational data are from stars, and these data can be applied in the study of systems of stars (galaxies, star clusters, etc.). Stellar population synthesis modeling is a widely utilized tool in this kind of study because the stellar population is the basic ingredient in a system of stars. Moreover, the integrated spectrum of a stellar population contains a large amount of effective information, so the calculation of integrated spectra is necessary for stellar population synthesis models.

In the widely used evolutionary population synthesis models (Bruzual & Charlot 2003; Mollá et al. 2009;

Zhang et al. 2013, etc.), the below three key components are incorporated for the integrated spectra of the stellar populations. 1. initial mass function (IMF), which provides the relative number for stars with an initial mass  $M$ ; 2. isochrone library, which is derived from the stellar evolution model and is used to give the stellar parameters (including the atmospheric parameters) for stars in a stellar population; 3. the stellar spectral library, which is utilized to convert the stellar atmospheric parameters to the stellar spectra. At last, the integrated spectrum of stellar population is the sum of the stellar spectrum.

The stellar spectral library gives a correspondence between the stellar atmospheric parameters and the spectrum. A stellar spectral library can be divided to t-

two kinds: theoretical and empirical libraries. The theoretical spectra are calculated from the stellar atmosphere model (Kurucz 1992; González Delgado et al. 2005, etc.), while the empirical spectra are from observations (Prugniel & Soubiran 2001; Le Borgne et al. 2003; Sánchez-Blázquez et al. 2006; Chen et al. 2014, etc.).

For the empirical and theoretical spectral libraries, each one has its own advantages and disadvantages. Because the theoretical spectra are calculated from the atmospheric model, and they have larger coverage in range of wavelength, spectral resolution and stellar atmospheric parameters. However, they are limited by the incomplete atomic- and molecular-line lists, the uncertain abundance pattern, the assumption and idealized treatment in the model calculation, and so on (Kurucz 2014). Unlike the theoretical spectral library, the empirical spectra are from observations, they have limited wavelength, resolution, noise and error that is increased from observation and data processing (e.g. flux calibration and stellar atmospheric parameter extraction). They avoid many disadvantages of the theoretical spectra. The theoretical and empirical stellar spectral libraries are complementary.

Because the stars in a spectral library are discrete, we need an interpolator to produce the spectra of any set of possible stellar atmospheric parameters. The distribution of stars in theoretical spectral libraries has less atmospheric parameter limitations and usually is dense and regular. Under this situation, the classical linear interpolation method can produce a reliable interpolation result. However, for the empirical stellar spectral library, the stars are discrete in the atmospheric parameter space, and this irregular distribution makes the traditional interpolator difficult to produce the expected interpolation results. Therefore, in the work of Cheng et al. (2018) we constructed an interpolator based on a radial basis function (RBF) network to get stellar spectra in the stellar population synthesis model. The algorithm is different from those using polynomial form (e.g. Wu et al. 2011 and Prugniel et al. 2011).

The interpolator based on the RBF network is called the RBF interpolator in this text. The computational formula for the RBF interpolator (Eq. (3)) is similar to the formula for a field in the smoothed particle hydrodynamics (SPH) simulation and the formula for the expected number in the likelihood estimation. All of them are based on calculations of the kernel functions. In this work, a Gaussian function is implemented as the kernel function as expressed in Equation (5), and the  $\sigma$  is the standard deviation used to characterize the effective region of the kernel function.

For the RBF interpolator, the kernel function does not have any strict constraint, and the different settings of the

kernel functions will influence the interpolation results. If all the Gaussian kernel functions have the same  $\sigma$ , a relatively small  $\sigma$  in the sparse area will make the interpolation results be discrete, however, a relatively large  $\sigma$  in the dense area will oversmooth the interpolation results (lack detailed information). In the work of Cheng et al. (2018), the local average distance is utilized to give the  $\sigma$  for the Gaussian kernel function. This is because the distribution of stars in the spectral library is non-homogeneous in the stellar atmospheric parameter space.

In this work, we compare the interpolation calculation of the RBF network with the calculation of the density field in SPHs. Under this comparison, we include a constraint about the  $\sigma$  in the Gaussian kernel function of RBF network from the relation between the smoothing length and the density in SPHs. Under this constraint, the size of  $\sigma$  for each kernel function is related to the local density of sample points in the parameter space. We apply this constraint to replace the coarse determination about  $\sigma$  in the work of Cheng et al. (2018) for the RBF network Gaussian kernel function. Moreover, same as in SPHs, the spherically symmetric kernel function usually is not a better selection (Bicknell & Gingold 1983; Shapiro et al. 1996; Owen et al. 1998). We will refer to the process of adaptive smoothed particle hydrodynamics (ASPH) simulation and take an anisotropic kernel function in the RBF interpolation calculations. As a result, we will present an upgraded RBF interpolator which can be employed for the spectral calculation based on the empirical stellar spectral library.

The outline of this paper is as follows. In Section 2, we briefly introduce the RBF network and its structure, then explain the constraint on the kernel function applied in this work and constructing the anisotropic kernel function in the RBF network. In Section 3, we implement the Beetle Antennae Search algorithm (Jiang & Li 2017, hereafter BAS) to search for the best kernel function parameters. In Section 4, we present the interpolation spectra and test this upgraded RBF interpolator by employing the medium-resolution Isaac Newton Telescope library of empirical spectra (hereafter MILES, Sánchez-Blázquez et al. 2006; Cenarro et al. 2007), and compare it with our previous work in Cheng et al. (2018). At last, in Section 5, we give the conclusion of this work.

## 2 METHOD

In the stellar population synthesis model, the stellar spectral library provides a fast way to get the spectra of any star compared with direct calculation by the stellar atmospheric model. This process is a fitting or an interpolation process of the spectra in the stellar atmospheric parameter space (usually it includes three parameters: effective temperature  $T_{\text{eff}}$ , logarithmic surface gravity acceleration  $\lg g$

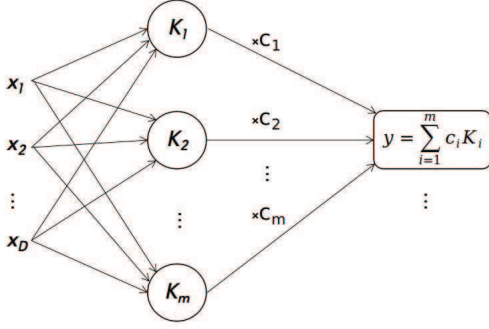


**Fig. 1** The three-layer structure of an RBF network is illustrated. The left part is the input layer and  $\mathbf{x}$  ( $x_1, x_2, \dots, x_D$ ) is the input sample coordinate in the  $D$ -dimensional space. The middle part is a hidden layer that is constituted by RBF functions  $K_i(\mathbf{x} - \boldsymbol{\mu}_i)$ ,  $i = 1, 2, 3, \dots, m$ ,  $\boldsymbol{\mu}_i$  ( $\mu_1, \mu_2, \mu_3, \dots, \mu_D$ ) $_i$  is the central coordinate of  $K_i(\mathbf{x} - \boldsymbol{\mu}_i)$  in the  $D$ -dimensional space and  $m$  is the number of RBF functions in the hidden layer. The right part is the output layer and  $y$  is the prediction value which is the sum of RBF function multiplied by the corresponding weight factor  $\mathbf{c}$  ( $c_1, c_2, c_3, \dots, c_m$ ).

and metallicity [Fe/H]). The stellar spectral library gives a correspondence between stellar atmospheric parameters and stellar spectra.

In this section, we will provide a detailed introduction of the RBF network and the upgraded RBF interpolator in our work. In Section 2.1, we explain the RBF network and its calculation process as an interpolator (RBF interpolator). In Section 2.2, we describe the kernel function of the upgraded RBF interpolator in our work. In Section 2.3, we give a summary of the upgraded RBF interpolator in our work.

## 2.1 RBF network and interpolator

An early introduction of RBF interpolator can be found in Powell (1987). Broomhead & Lowe (1988) introduced the RBF into an artificial neural network (ANN) framework. Up to now, the RBF interpolation and fitting method has been applied widely in many fields (such as mineral analysis, aircraft design, image processing and pattern classification).

An RBF interpolator can be thought as an application of an RBF network which is a kind of kernel method. An RBF is also called a kernel function in this paper. The construction of an RBF network is diagrammed in Figure 1. Moreover, the sample in this work is a set of points with the coordinate set  $\{\mathbf{x}_1, \mathbf{x}_2, \dots, \mathbf{x}_i, \dots, \mathbf{x}_N\}$  and the values  $\{y_1, y_2, \dots, y_i, \dots, y_N\}$  ( $\mathbf{x}_i$  ( $x_1, x_2, \dots, x_D$ ) $_i$  are the  $i$ th sample point coordinate in  $D$ -dimensional space. In this paper, we use  $\{\}$  to represent a set in mathematics.

From Figure 1, we can find the RBF network consists of three layers. The left is the input layer and

$\mathbf{x}$  ( $x_1, x_2, \dots, x_D$ ) is the input point coordinate. The middle is the hidden layer which is constituted by kernel functions  $K_i(\mathbf{x} - \boldsymbol{\mu}_i)$  ( $i = 1, 2, \dots, m$ ) and  $\boldsymbol{\mu}_i$  ( $\mu_1, \mu_2, \mu_3, \dots, \mu_D$ ) $_i$  is the central coordinate of the  $i$ th kernel function in  $D$ -dimensional space. The right is the output layer which is the sum of the kernel function multiplied by the weight factor ( $y = \sum_{i=1}^m c_i \cdot K_i(\mathbf{x} - \boldsymbol{\mu}_i)$ ) and the size of the output layer has no limitation. In the spectral interpolation,  $y$  is the flux within a given wavelength interval. It is a one-dimensional scalar, and the interpolation spectrum consists of the interpolated fluxes at different wavelengths.

For a sample with a huge size ( $N$ ), a fast RBF network can be constituted by a much smaller number of kernel functions in the hidden layer ( $m \ll N$ ). Usually, the K-means clustering method (MacQueen 1967; Ding & He 2004) is used to search for the kernel central coordinates  $\boldsymbol{\mu}_i$  ( $i = 1, 2, 3, \dots, m$ ), then a linear regression method is applied to get the weight factor array  $\mathbf{c}$  ( $c_1, c_2, c_3, \dots, c_m$ ) for the sample set  $\{(\mathbf{x}, y)_i, i = 1, 2, 3, \dots, N\}$ .

The empirical stellar spectral library usually comprises several hundred or thousands of spectra. So in our work, the number of kernel functions  $m$  is set to be same as the sample number  $N$ . Moreover, we do not need the calculations with K-means and the linear regression. We take the sample points as the centers of the kernel functions directly in the spectral RBF interpolator ( $\boldsymbol{\mu}_i = \mathbf{x}_i$ ,  $i = 1, 2, 3, \dots, N$ ). The weight factor array  $\mathbf{c}$  of the kernel function in the hidden layer is obtained by solving the system of linear equations

$$\sum_{j=1}^N K_j(\mathbf{x}_i - \mathbf{x}_j) \cdot c_j = y_i \quad (i = 1, 2, 3, \dots, N). \quad (1)$$

In our works, the Gaussian kernel function  $e^{-\sum_{d=1}^D (x_d - \mu_d)^2 / (2\sigma^2)}$  is utilized,

$$K_j(\mathbf{x}_i - \mathbf{x}_j) = e^{\frac{-\sum_{d=1}^D (x_{d,i} - x_{d,j})^2}{2\sigma_j^2}}, \quad (2)$$

where  $x_{d,i}$  and  $x_{d,j}$  are the coordinates of the  $i$ th and  $j$ th sample point in the  $D$ -dimensional space ( $d = 1, 2, 3, \dots, D$ ). The central coordinate of the  $j$ th kernel function  $K_j$  is  $\mathbf{x}_j$ , and  $\sigma_j$  is the standard deviation of the  $j$ th kernel function  $K_j$  which can be applied to characterize the influence range of the kernel function.  $c_j$  is the weight factor of the  $j$ th Gaussian kernel function. Solving the linear Equation (1), we can arrive at the weight factor array  $\mathbf{c}$ , if sample coordinates in set  $\{\mathbf{x}_1, \mathbf{x}_2, \mathbf{x}_3, \dots, \mathbf{x}_N\}$  are different from each other<sup>1</sup>. After obtaining  $\mathbf{c}$ , we can get a simple formula for the interpolation calculation,

$$y(\mathbf{x}) = \sum_{j=1}^N K_j(\mathbf{x} - \mathbf{x}_j) \cdot c_j, \quad (3)$$

<sup>1</sup> For a Gaussian kernel function, this conclusion can get a fixed factor array  $\mathbf{c}$  from the Micchelli theorem (Micchelli 1986)

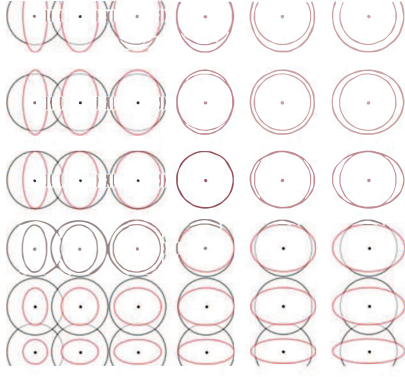


**Fig. 2** A example of the 2D spatial  $\sigma$  distribution for the kernel function. Black points are the centers of the kernel functions ( $\{\mu_i, i = 1, 2, 3, \dots, m\}$ ). From left to right and from bottom to top, the density of points decreases. The radius of black rings characterize the  $\sigma$  influence range for the classical RBF network. Red ellipses characterize a more reasonable influence range of kernel functions for anisotropic distribution.

where  $\mathbf{x}$  is the input coordinate and  $y(\mathbf{x})$  is the interpolation result. For spectral interpolation calculation,  $\mathbf{x}$  and  $y$  correspond to the stellar atmospheric parameter and the interpolated flux within a wavelength interval, respectively.

The RBF network is based on the kernel functions. However, a constant  $\sigma$  is usually used for all the Gaussian kernel functions (Lowe 1989). For the irregular distribution of stars in the stellar spectral library, the choice of all the kernel functions having the same  $\sigma$  is not a better selection. Next, we will introduce the kernel function in our spectral RBF interpolator.

## 2.2 Gaussian kernel function in the upgraded RBF interpolator

The constant  $\sigma$  in the Gaussian kernel functions has a disadvantage: large  $\sigma$  for the kernel function makes the interpolation results oversmoothed in a dense area, and a relatively small  $\sigma$  makes the interpolation results discrete in a sparse area. In Figure 2, we present an example of a two-dimensional (2D)  $\sigma$  distribution, in which the black points are the centers of the kernel functions  $\{\mu_i, i = 1, 2, 3, \dots\}$ , and the spatial density decreases from left to right and bottom to top, and an anisotropic distribution exists in the top-left and bottom-right parts. The black rings characterize the influence range of kernel functions in the traditional RBF network and the red ellipses signify a better choice for the anisotropic kernel functions.

Stars in the empirical spectral library face a more complex situation than Figure 2. The distribution is nonuniform and its density varies significantly in the stellar atmospheric parameter space (a typical situation can be found

in Figure 3). This situation results from observational and theoretical limitations<sup>2</sup>. In our work, we set a constraint by including a relation between the  $\sigma$  and the spatial density of sample points in the RBF network, and this relation can be used to determine the  $\sigma$  value. Moreover, we also consider the anisotropy of the kernel function in the RBF network by referring to the ASPHs.

In Section 2.2.1, we give an introduction to the constraint on  $\sigma$ . In Section 2.2.2, we show generic Gaussian kernel function for the anisotropic situation in our works.

### 2.2.1 The constraint on $\sigma$ and its size calculation

In this part, we introduce the smoothing length constraint of SPHs into the RBF network. Under this constraint, we explain the computing method of  $\sigma$  for the kernel function in the RBF network.

In the SPHs, the sample consists of particles with the coordinate set  $\{\mathbf{x}_i, i = 1, 2, 3, \dots, N\}$  and mass set  $\{m_i, i = 1, 2, 3, \dots, N\}$ , in which  $\mathbf{x}_i$  and  $m_i$  are the position and mass of the  $i$ th particle respectively. The fluid density  $\rho$  in the position  $\mathbf{x}_i$  is

$$\rho_i \approx \sum_{j=1}^N m_j \cdot W_{ij} \quad (i = 1, 2, 3, \dots, N), \quad (4)$$

where  $N$  is the number of particles,  $W_{ij}$  is  $a \cdot K(\mathbf{x}_i - \mathbf{x}_j)$  and  $a$  is the normalized coefficient. We utilize the Gaussian kernel function

$$W_{ij} = \frac{1}{(\sqrt{2\pi}\sigma_j)^D} \cdot e^{-\frac{\sum_{d=1}^D (x_{d,i} - x_{d,j})^2}{2 \cdot \sigma_j^2}}, \quad (5)$$

where  $D$  is the spatial dimension and  $\sigma_j$  is the smoothing length of the  $j$ th kernel function. Replacing  $m_j$  with  $\rho_j V_j$ , where  $V_j$  is the volume of the  $j$ th particle in SPHs, we have

$$\rho_i \approx \sum_{j=1}^N \rho_j \cdot V_j \cdot W_{ij} = \sum_{j=1}^N \rho_j \cdot V_j \cdot \frac{1}{(\sqrt{2\pi}\sigma_j)^D} \cdot e^{-\frac{\sum_{d=1}^D (x_{d,i} - x_{d,j})^2}{2 \cdot \sigma_j^2}}. \quad (6)$$

The fluid density varies with time. A better smoothing length should vary dynamically. Usually,  $\sigma = \sigma_0 \cdot (\rho_0/\rho)^{1/D}$  is utilized to give the current smoothing length ( $\sigma_0$  and  $\rho_0$  are initial values of SPHs). This relation yields a constraint on the  $\sigma$  by spatial density of sample points. Here, we apply this relation in the kernel function of the

<sup>2</sup> For spectroscopic observations, only solar neighborhood stars can be observed with high quality. In stellar theory, the bright stars allows having a short evolutionary time scale. Both of them make the observed spectral sample have an obvious selection effect

RBF network at different positions (in the stellar atmospheric parameter space). We provide the constraint about  $\sigma$ ,

$$\sigma \propto \rho^{-\frac{1}{D}} \propto V^{\frac{1}{D}}, \quad (7)$$

where  $V$  is used to characterize the particle volume which is related to the influence range of the kernel function. Usually, the dimension number  $D$  is 3 for the stellar spectral library.

Now, including the constraint (formula (7)) in Equation (6), we have

$$\rho_i \approx \sum_{j=1}^N \rho_j \cdot \frac{c_0}{(\sqrt{2\pi})^D} \cdot e^{-\frac{\sum_{d=1}^D (x_{d,i} - x_{d,j})^2}{2 \cdot \sigma_j^2}} \quad (i = 1, 2, 3, \dots, N), \quad (8)$$

where  $c_0 \equiv V/(\sigma^D)$ . Equation (8) yields a set of nonlinear equations for  $\sigma$ . However, they are difficult to solve.

To simplify Equation (8), we approximate Equation (8) to the following expression by replacing  $j$  with  $i$  for the subscripts of  $\sigma$  and  $\rho$ ,

$$1 \approx \sum_{j=1}^N \frac{c_0}{(\sqrt{2\pi})^D} \cdot e^{-\frac{\sum_{d=1}^D (x_{d,i} - x_{d,i})^2}{2 \cdot \sigma_i^2}} \quad (i = 1, 2, 3, \dots, N). \quad (9)$$

This is because  $\rho$  and  $\sigma$  are continuous and the adaptive kernel function (here, it is a Gaussian function) is for a local region. The terms in the equation become independent of each other. From Equation (9), we can apply the bisection method to calculate  $\sigma_i$  ( $i = 1, 2, 3, \dots, N$ ) quickly. In this process, the  $\sigma$  can be adjusted by the control parameter  $c_0$ . From Equation (9), we can know  $c_0$  is within the interval of  $((2\pi)^{D/2}/N, (2\pi)^{D/2}]$ , and its upper and lower limits correspond to  $\infty$  and 0 respectively for  $\sigma$ .

In Figure 3, we display the resulting  $\sigma_i$  ( $i = 1, 2, 3, \dots, N$ ) for the dimensionless stellar atmospheric parameter of the MILES library. In this work, the coordinates ( $T_{\text{eff}}$ ,  $\lg g$ ,  $[\text{Fe}/\text{H}]$ ) are dimensionless which are expressed in the units of mean squared error (hereafter MSE). The size of  $\sigma$  is relatively large in the sparse area and small in the dense area.

We should also notice that the  $\sigma_i$  in Equation (9) is a scalar, which corresponds to the isotropic kernel function. In fact, the anisotropic distribution of stars in the stellar atmospheric parameter space is common for the empirical spectral library (displayed in Fig. 3).

### 2.2.2 Anisotropic Gaussian kernel function

This part gives the introduction of the anisotropic kernel function by generalizing the Gaussian kernel function.

In SPHs, the fluid varies with time and the deformation usually is not isotropic. For an anisotropic deformation, the isotropic kernel function usually is not able to give

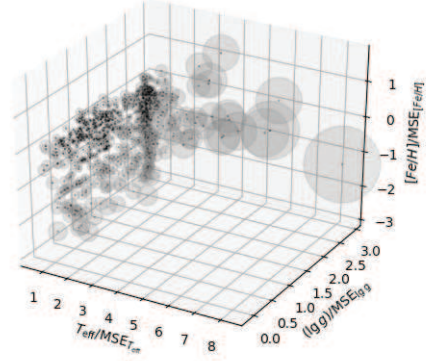


**Fig. 3** The size of  $\sigma$  in the kernel function for the MILES stellar spectral library. The coordinates of black points are the dimensionless stellar atmospheric parameters of the MILES library ( $T_{\text{eff}}/\text{MSE}_{T_{\text{eff}}}$ ,  $(\lg g)/\text{MSE}_{\lg g}$  and  $[\text{Fe}/\text{H}]/\text{MSE}_{[\text{Fe}/\text{H}]}$ , and the MSE is the mean squared error function). The radius of semitransparent spheres around black points characterizes the corresponding  $\sigma$ .

a better smoothing effect as shown in Figure 2. Similarly, Bicknell & Gingold (1983) have even considered a kernel function with different smoothing lengths in the  $y$  and  $z$  axis directions in a tidal destr simulation. Moreover, the generalized anisotropic kernel function has been discussed by Shapiro et al. (1996) and Owen et al. (1998).

The anisotropic kernel function is the generalization of the isotropic Gaussian kernel function. If we let  $M_{\text{iso}}^2$  be  $\sum_{d=1}^3 (x_d - \mu_d)^2 / (2\sigma^2)$ , which is the exponential part of the isotropic Gaussian kernel function, then the corresponding vector  $M_{\text{aniso}}$  of anisotropic kernel function can be described by the following

$$\begin{aligned} M_{\text{aniso}} &= \mathbf{T} \cdot (\mathbf{x} - \boldsymbol{\mu}) = \sum_{k=1}^3 T_{dk} \cdot (x_k - \mu_k) \quad (10) \\ &= \begin{bmatrix} T_{11} & T_{12} & T_{13} \\ T_{21} & T_{22} & T_{23} \\ T_{31} & T_{32} & T_{33} \end{bmatrix} \begin{bmatrix} x_1 - \mu_1 \\ x_2 - \mu_2 \\ x_3 - \mu_3 \end{bmatrix} \\ &= \begin{bmatrix} Z_{11} & 0 & 0 \\ 0 & Z_{22} & 0 \\ 0 & 0 & Z_{33} \end{bmatrix} \begin{bmatrix} R_{11} & R_{12} & R_{13} \\ R_{21} & R_{22} & R_{23} \\ R_{31} & R_{32} & R_{33} \end{bmatrix} \begin{bmatrix} x_1 - \mu_1 \\ x_2 - \mu_2 \\ x_3 - \mu_3 \end{bmatrix} \\ &(d = 1, 2, 3), \end{aligned}$$

where  $d$  and  $k$  are the dimensional subscripts, and the matrix  $\mathbf{T}$  is a linear translation (from  $\mathbf{x} - \boldsymbol{\mu}$  to  $M_{\text{aniso}}$ ). The generalized Gaussian kernel function result can be written as  $e^{-M_{\text{aniso}}^2}$ .

Matrix  $\mathbf{T}$  can be separated into two parts  $\mathbf{T} = \mathbf{Z} \cdot \mathbf{R}$  as is evident in Equation (10). The diagonal matrix  $\mathbf{Z}$  is utilized to provide a scaled transformation along the axis, the matrix  $\mathbf{R}$  is constituted by three orthogonal bases and preforms a rotational transformation. Both  $\mathbf{Z}$  and  $\mathbf{R}$  change with the position of kernel function center  $\boldsymbol{\mu}$  in the stellar atmospheric parameter space. The isotropic kernel

function can be recovered by setting  $\mathbf{I} = \mathbf{R} = \sqrt{2\sigma} \cdot \mathbf{Z}$ , where  $\mathbf{I}$  is an identity matrix.

In the stellar spectral library, most stars are distributed along the main sequence and in the red giant region. These two parts are distributed almost along the  $T_{\text{eff}}$  and  $\lg g$  axis directions, and the distribution of stars in different  $[\text{Fe}/\text{H}]$  ranges only have a slight bias. Therefore, in most cases, the anisotropy is in the axis direction. To simplify the calculation process, in this work we ignore the rotational matrix  $\mathbf{R}$  by setting  $\mathbf{R} = \mathbf{I}$  and only consider  $Z_{11}$ ,  $Z_{22}$  and  $Z_{33}$  in the generic Gaussian kernel function.

The degree of anisotropy for the kernel function is dependent on the ratio of  $Z_{11}$ ,  $Z_{22}$  and  $Z_{33}$ . In our work, the axial local dispersion  $\mathbf{D}$  is used to give the  $\tilde{\mathbf{Z}}$  for any kernel function with central coordinate  $\boldsymbol{\mu}$ ,

$$Z_{dd} \propto \tilde{Z}_{dd} = c_1 + \frac{(1 - c_1)D_d}{(\sum_{d=1}^3 D_d^2)^{1/2}} \quad (d = 1, 2, 3),$$

$$D_d = \sqrt{\sum_{i=1}^N (x_{d,i} - \mu_d)^2 \cdot e^{-\frac{\sum_{d=1}^3 (x_{d,i} - \mu_d)^2}{2\sigma^2}}}$$
(11)

where  $c_1$  is a control parameter which is utilized to adjust the degree of anisotropy and the Gaussian function is employed to limit the calculation in the local region. So after the calculation of Equation (11), we can know the ratio of  $Z_{11}$ ,  $Z_{22}$  and  $Z_{33}$  in the matrix  $\mathbf{Z}$  for all kernel functions and get the corresponding normalized matrix  $\tilde{\mathbf{Z}}$ . The last  $\mathbf{Z}$  is obtained by solving the Equation (9) again with the anisotropic kernel function  $e^{-[\tilde{\mathbf{Z}}(\mathbf{x}-\boldsymbol{\mu})]^2}$ .

### 2.3 Summary of the method

Here, we provide a summary of the mathematical process of the RBF interpolator in this work. In general, as illustrated in Figure 1, there are two key parts for the RBF network that need to be considered, one is the kernel functions  $\{K_1, K_2, K_3, \dots, K_N\}$ , the other is the coefficients array  $c$ . For the latter,  $c$  can be obtained by solving the system of linear equations (1) for the given kernel functions and the sample  $\{(\mathbf{x}, y)_i, i = 1, 2, 3, \dots, N\}$ . Next, we will list the determination process of the RBF kernel functions  $\{K_1, K_2, K_3, \dots, K_N\}$ .

First of all, we use the stellar spectral library as the sample of the RBF network,  $\{\mathbf{x}_1, \mathbf{x}_2, \mathbf{x}_3, \dots, \mathbf{x}_N\}$  corresponds to the stellar atmospheric parameters and  $\{y_1, y_2, y_3, \dots, y_N\}$  corresponds to the flux. We select the Gaussian kernel function and set the central coordinates of all kernel functions as the coordinates of the sample ( $\boldsymbol{\mu}_i = \mathbf{x}_i, i = 1, 2, 3, \dots, N$ ). Next, for the  $i$ th kernel function ( $i = 1, 2, 3, \dots, N$ ), three steps will be executed.

1. Solving Equation (9) to get  $\sigma_{\text{iso},i}$  of the isotropic Gaussian kernel function. In this step, we include parameter  $c_0$  for all points.
2. Inputting  $\sigma_{\text{iso},i}$  in Equation (11) and calculating the matrix  $\tilde{\mathbf{Z}}_i$ . In this step,  $c_1$  is utilized to control the degree of anisotropy of kernel functions.
3. Rewriting the exponential part of Equations (9) by  $e^{-[\tilde{\mathbf{Z}}(\mathbf{x}-\boldsymbol{\mu})]^2}$  and solving it, we can obtain the last  $\mathbf{Z}_i$  and  $\mathbf{T}_i$  (in this step, a new parameter  $c_2$  is included which corresponds to  $c_0$  in the first step).

After those three steps, we arrive at the last kernel function of the RBF network, then solve the system of Equations (1) to obtain the weight factor array  $c$ . At last, we get the last RBF network, and the calculation of spectral RBF interpolator corresponds to Equation (3).

The three control parameters  $c_0, c_1, c_2$  are included, and the optimization calculation of these parameters is shown below. For distinguishing the RBF interpolator in Cheng et al. (2018) from that in this work, we name these two spectral RBF interpolators RBF18 and RBF<sub>update</sub>.

### 3 OPTIMIZING THE RBF NETWORK CONTROL PARAMETERS

We can control the RBF network by adjusting the control parameters ( $c_0, c_1, c_2$ ) (Section 2.3). In this section, we will introduce the optimization process of these three control parameters.

In this work, the MILES library is applied to build the spectral RBF interpolator RBF<sub>update</sub>. The MILES empirical stellar spectral library includes  $\sim 1000$  stars obtained with the 2.5 m Isaac Newton Telescope. The wavelength ranges from 3540.5 to 7409.6 Å and the spectral resolution is  $\sim 2.3$  Å (Sánchez-Blázquez et al. 2006, FWHM). The coverage of the stellar atmospheric parameters is:  $2748 < T_{\text{eff}} < 36000$  K,  $0.00 < \lg g < 5.50$  and  $-2.93 < [\text{Fe}/\text{H}] < +1.65$ . The MILES spectral library has a larger coverage in the parameter spaces than the other empirical stellar spectral libraries used in the stellar population synthesis models (Cenarro et al. 2007).

In this work, we utilize the semi-empirical BaSeL-3.1 stellar spectral library (Lejeune et al. 1997, 1998; Westera et al. 2002) as the reference library to find the best control parameters of the RBF<sub>update</sub> interpolator. BaSeL-3.1 is one of the widely used spectral libraries. It provides an extensive and homogeneous grid of low-resolution spectra in the range of  $91 - 1\,600\,000$  Å for a large range of stellar parameters:  $2000 < T_{\text{eff}} < 50\,000$  K;  $-1.02 < \lg g < 5.5$  and  $-5.0 < [\text{Fe}/\text{H}] < 1.0$ .

For avoiding extrapolation of the spectral RBF interpolator, the input parameter should be within the coverage area of stars in the MILES library. So in the BaSeL-

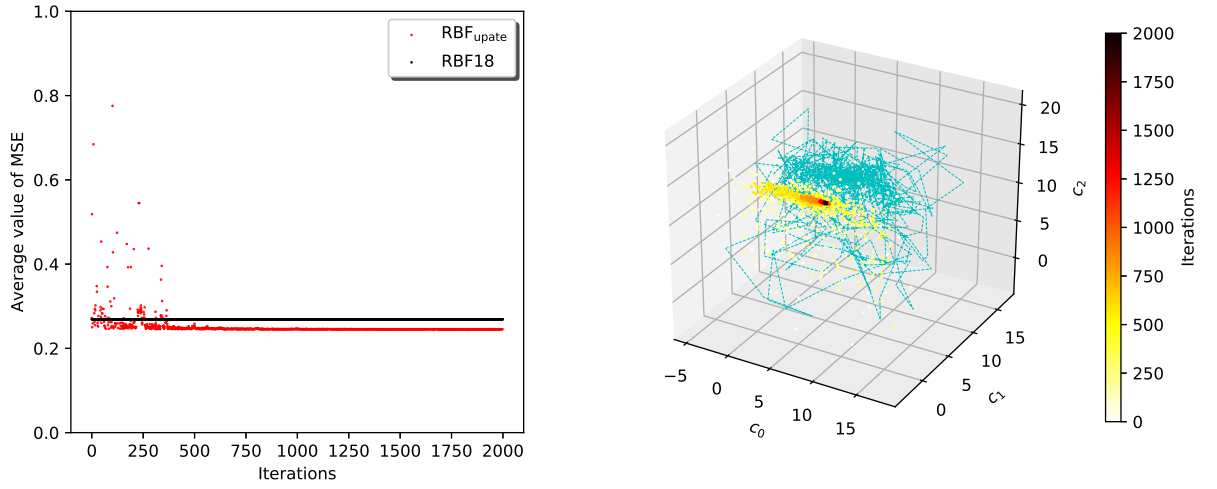


**Fig. 4** The output of the optimization process by the BAS search algorithm. The left panel displays the variation of object function as a function of the iteration times. Red points are the objective function values of the RBF<sub>update</sub> interpolator. Black points are the objective function values of the RBF18 interpolator which is utilized as a comparison. The right panel depicts the corresponding track of the point  $(c_0, c_1, c_2)$ . The cyan dashed line is displacement, and nodes are the coordinates of  $(c_0, c_1, c_2)$  at different iterations. The node color corresponds to the number of iterations, and 2000 iterations are shown here.

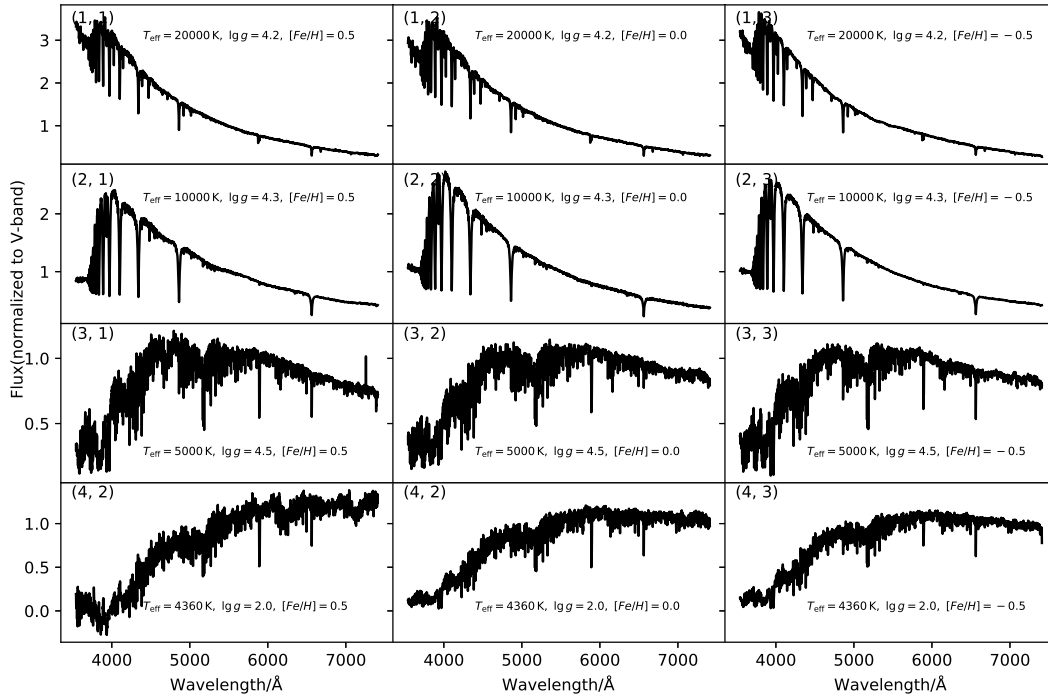


**Fig. 5** The 12 interpolated spectra based on the MILES spectral library by the RBF<sub>update</sub> interpolator. Input stellar parameters are expressed in each panel. Here the spectra are dimensionless. The first two lines show the interpolated spectra of six main sequence stars with  $T_{\text{eff}} = 20\,000\text{ K}$  and  $T_{\text{eff}} = 10\,000\text{ K}$ . The third line features the interpolated spectra of three main sequence stars with  $T_{\text{eff}} = 5000\text{ K}$ . The fourth line showcases the interpolated spectra of three red giant stars with  $T_{\text{eff}} = 4360\text{ K}$ . In each line, the input stellar metallicity is  $[\text{Fe}/\text{H}] = 0.5, 0.0$  and  $-0.5$ .

3.1 library, only those models within the coverage area of MILES library are used here. A Gaussian smoothing algorithm is applied to degrade the resolution of the output spectra to  $20 \text{ \AA}$  (the resolution of BaSeL-3.1 in visible wavelength). Iterative calculation is employed in the optimization. In each iteration, hundreds of stars in BaSeL-3.1 are selected as the input sample, and the output interpolation spectra are utilized to compare with the original spectra in BaSeL-3.1. The average value of the mean squared error between interpolated spectra and original spectra in BaSeL-3.1 is implemented as an objective function  $f(c_0, c_1, c_2)$  in the optimization process, and the best  $(c_0, c_1, c_2)$  corresponds to the minimum of  $f(c_0, c_1, c_2)$ .

Many widely used optimization algorithms need massive computational capability to obtain the best  $(c_0, c_1, c_2)$ . BAS algorithm is selected (Jiang & Li 2017), which is a new and light algorithm by simulating the beetle behavior. In this work, the process of the BAS search is in three-dimensional (3D) space of  $(c_0, c_1, c_2)$  and comprises four steps.

- Step1. Setting the initial position of the ‘beetle’  $\mathbf{P}_0$ , the initial distance of two antennas  $A_0$  and the initial step length  $S_0$ . For the  $i$  th iteration, it is referred to as  $\mathbf{P}_i$ ,  $A_i$ ,  $S_i$ ;
- Step2. Generating a unit vector  $\mathbf{d}$  with random direction,  $\mathbf{d}$  is used to give the relative position of two antennas. Then, the left antenna position has  $\mathbf{P}_{l,i} = \mathbf{P}_i - 0.5 \cdot A_i \cdot \mathbf{d}$ , and the right antenna position has  $\mathbf{P}_{r,i} = \mathbf{P}_i + 0.5 \cdot A_i \cdot \mathbf{d}$ ;
- Step3. Calculating the objective function on two antennas  $f(\mathbf{P}_{l,i}), f(\mathbf{P}_{r,i})$ . The new position is  $\mathbf{P}_{\text{new}} = \mathbf{P}_i + [f(\mathbf{P}_{r,i}) - f(\mathbf{P}_{l,i})] / \text{abs}(f(\mathbf{P}_{r,i}) - f(\mathbf{P}_{l,i})) \cdot \mathbf{d} \cdot S_i$ ;
- Step4. If an iteration meets the critical condition, the process jumps out of the iterations. If not,  $i + 1 = i$ ,  $\mathbf{P}_i = \mathbf{P}_{\text{new}}$  and the loop goes back to Step2.

During iteration, the distance between the two antennas  $A_i$  and the step length  $S_i$  changes slowly. In our calculation,  $S_{i+1} = b \cdot S_i$  and  $A_i = c \cdot S_i$ ,  $b$  is a constant coefficient close to 1 but less than 1 and  $c$  is also a constant coefficient.

Figure 4 depicts the iteration process of the  $(c_0, c_1, c_2)$  in the optimization. In this figure, 2000 iterations are shown. The left panel displays the objective function output, in which red points are the objective function values of the RBF<sub>update</sub> interpolator. As a comparison, the black points are the objective function value of the RBF18 interpolator in the same calculation. In the right panel, the cyan dashed line traces the movement trail of the ‘beetle’, and the color nodes are the ‘beetle’ positions at different iterations. The node color corresponds to the number of iterations. We can find the result of  $(c_0, c_1, c_2)$  converges to a fixed value at last. The objective function of the RBF<sub>update</sub>

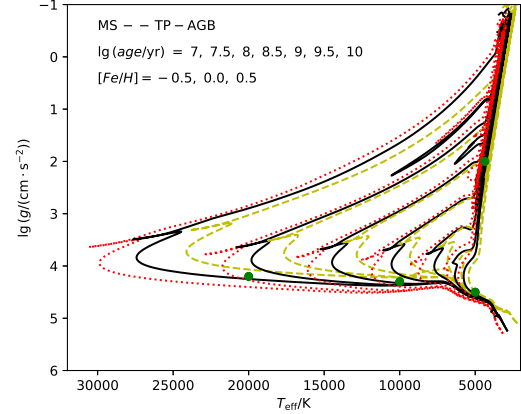


**Fig. 6** The positions (green points) of the stars in Figure 5. The isochrones are used to give the relative position. For each isochrone, stars from the zero-age main sequence to the end of TP-AGB phases are displayed. The red dotted lines have  $[\text{Fe}/\text{H}] = -0.5$ , black lines have  $[\text{Fe}/\text{H}] = 0$  and green dashed lines have  $[\text{Fe}/\text{H}] = 0.5$ . From left to right  $\lg(\text{age}/\text{yr})$  are 7, 7.5, 8, 8.5, 9, 9.5 and 10 respectively.

interpolator is lower than the result of the RBF18 interpolator. This means that spectral interpolator RBF<sub>update</sub> has a better performance than RBF18 in the spectral interpolation calculation of stars in the BaSeL-3.1 library.

## 4 RESULT AND ANALYSIS

In this section, we provide the interpolation results and the analysis of RBF<sub>update</sub> interpolator based on the empirical stellar spectral library MILES. In Section 4.1, we present the interpolated stellar spectra for different spectral types. In Section 4.2, we give a test of the RBF<sub>update</sub> interpolator and compare the interpolated spectra by RBF<sub>update</sub> and RBF18 interpolators based on the MILES stellar spectral library. In Section 4.3, we give an analysis and a discussion for the behavior of the RBF<sub>update</sub> interpolator in our test.

### 4.1 Results

For the sake of clarity, we only show the interpolated spectra of 12 stars with typical stellar atmospheric parameters in Figure 5. All of the interpolated spectra are normalized to their  $V$ -band flux. The 12 panels are divided into four rows, and each row corresponds to three input stars with different metallicities  $[\text{Fe}/\text{H}] = -0.5, 0$  and  $0.5$  (the corresponding atmospheric parameters are depicted in each panel). In the first row, the input stars with  $T_{\text{eff}} = 20\,000 \text{ K}$  and  $\lg g = 4.2$  correspond to massive main-sequence stars and have a great effect on the  $U$ -band flux of the stellar population integrated spectra with stellar population age less than  $10^{7.5} \text{ yr}$ . In the second row, the input stars with

$T_{\text{eff}} = 10\,000\text{ K}$  and  $\lg g = 4.3$  correspond to medium mass main-sequence stars and have a great effect on the  $B$ -band flux of integrated spectra with stellar population age less than  $10^{8.5}\text{ yr}$ . In the third row, the input stars with  $T_{\text{eff}} = 5000\text{ K}$  and  $\lg g = 4.5$  correspond to a large number of low-mass main-sequence stars in the stellar population. They have a significant effect on the integrated  $V$ -band spectra of the stellar populations. In the last row, the input stars with  $T_{\text{eff}} = 4360\text{ K}$  and  $\lg g = 2.0$  correspond to red giant stars. They are very bright and have a great effect on the infrared band flux of the older stellar population's integrated spectra.

In Figure 6, we plot the positions of these stars (in Fig. 5) on the  $T_{\text{eff}}$  and  $\lg g$  plane (the green points). Moreover, we present three sets of isochrones at metallicity  $[\text{Fe}/\text{H}] = -0.5, 0$  and  $0.5$  to give the locations of the stellar populations. For each set of isochrones, from left to right the stellar ages are  $\lg(\text{age}/\text{yr}) = 7, 7.5, 8, 8.5, 9, 9.5$  and  $10$  respectively. The isochrones only show stars from the zero-age main sequence phase to the end of thermally pulsing asymptotic giant branch (TP-AGB) phase. The relative positions between stars and isochrones correspond to the above analysis of Figure 5. In this figure, the isochrones are the results of MIST (Dotter 2016; Choi et al. 2016). They are calculated by employing the stellar evolution code MESA (Paxton et al. 2011, 2013, 2015, 2018).

## 4.2 Tests and comparison

In this part, we test the  $\text{RBF}_{\text{update}}$  interpolator based the empirical spectral library MILES in Section 4.2.1, and we provide a comparison between the  $\text{RBF}_{\text{update}}$  and  $\text{RBF18}$  interpolators in Section 4.2.2.

### 4.2.1 Test of the $\text{RBF}_{\text{update}}$ interpolator

We test the  $\text{RBF}_{\text{update}}$  interpolator based on the MILES stellar spectral library. In the test, we delete one member star from the MILES stellar spectral library and use the remaining spectra as a library to calculate the spectrum of the deleted star. Every star in the MILES library has been tested by the above process, and the comparison between interpolated and original spectra is utilized to investigate the interpolation performance of the  $\text{RBF}_{\text{update}}$  interpolator (the same test is also done for the spectral interpolator  $\text{RBF18}$ ).

The MSE between interpolated and original spectra is employed to characterize the difference,  $\text{MSE} = \sqrt{\sum_{\lambda} (f_{\text{int}, \lambda} - f_{\text{ori}, \lambda})^2 / \text{len}(f_{\text{ori}, \lambda})}$ , where  $f_{\text{int}, \lambda}$  and  $f_{\text{ori}, \lambda}$  are the normalized flux on the  $\lambda$ th wavelength interval of the interpolated and original spectra, respectively, and  $\text{len}(f_{\text{ori}, \lambda})$  is the array length of the spectrum. Every

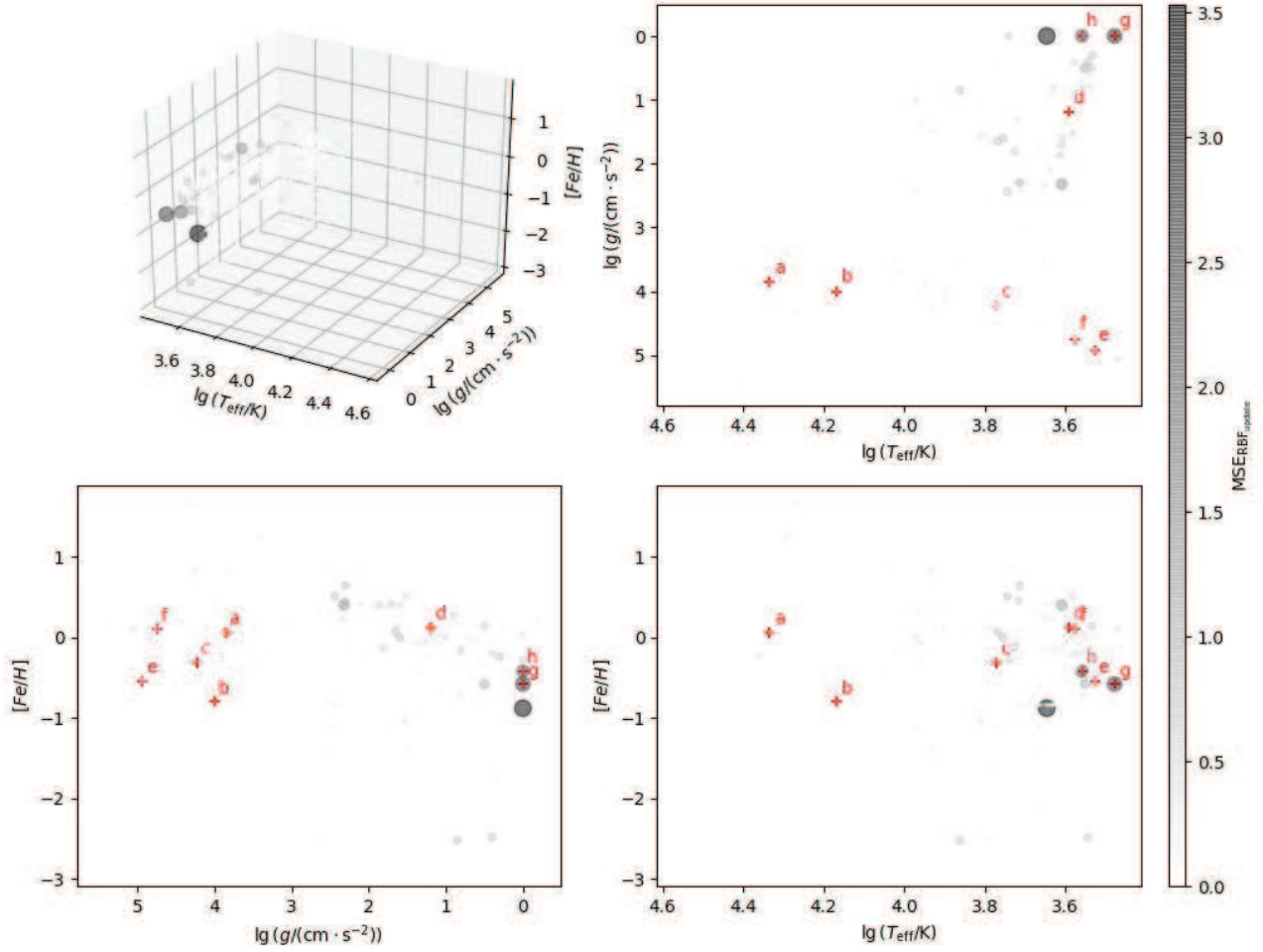
star in the MILES library has a corresponding MSE value, which we present in Figure 7.

Figure 7 plots the overall result of the MSE distribution. The top-left panel displays the result in the  $\lg T_{\text{eff}}, \lg g, [\text{Fe}/\text{H}]$  space. For the sake of clarity, the top-right panel features the projection of MSE on the  $\lg T_{\text{eff}}$  and  $\lg g$  plane, the bottom-left panel depicts the projection on the  $\lg g$  and  $[\text{Fe}/\text{H}]$  plane and the bottom-right panel showcases the projection on the  $\lg T_{\text{eff}}$  and  $[\text{Fe}/\text{H}]$  plane. For each panel, the MSE value is characterized by the gray level and point size. We can find that most stars have relatively small MSE values. An obvious difference exists in parts of the lower-temperature region, especially for stars at the edge of the low-metallicity red giant region.

For a more detailed analysis of the  $\text{RBF}_{\text{update}}$  interpolator, eight representative stellar spectra are shown in Figure 8 (the positions of those eight test stars are marked by red “+” symbols in Figure 7). In each panel of Figure 8, black lines are the original spectrum of the test star, and the green and red translucent lines are the interpolated spectra of the test star by  $\text{RBF}_{\text{update}}$  and  $\text{RBF18}$  interpolators, respectively. The interpolated spectra of the  $\text{RBF}_{\text{update}}$  interpolator and a copy of the original spectrum are moved upwards for the reason of clarity. The stellar atmospheric parameters and the MSE value also are expressed in each panel. Here the combination of green and black spectra provides the direct spectral performance of the  $\text{RBF}_{\text{update}}$  interpolator, and the combination of red and black spectra gives the direct spectral performance of the  $\text{RBF18}$  interpolator. Panels (a-d) list the representative spectra of massive main sequence, medium mass main sequence, low-mass main sequence and red giant test stars. We can find the interpolated spectra have a good match with the original spectra. Most of the test stars have similar results in our test, but there are still a few test stars that have bad test results. Panels (e-h) display four typical spectra that exhibit bad performance by  $\text{RBF}_{\text{update}}$  and  $\text{RBF18}$  interpolators. They are in the red giant (g-h) and low-mass main sequence (e-f) regions. This bad performance will be discussed in Section 4.3.

### 4.2.2 Comparison with $\text{RBF18}$ interpolator

In this section, we give a comparison between the  $\text{RBF}_{\text{update}}$  and  $\text{RBF18}$  interpolators by the test in Section 4.2.1. For any test star in the MILES library, we use the  $\text{MSE}_{\text{RBF}_{\text{update}}} - \text{MSE}_{\text{RBF18}}$  to characterize the discrepancy. The mean squared error MSE is larger than zero, and the smaller value of MSE means a better match between the interpolated and original spectra of a test star in the MILES library. So, the negative value of  $\text{MSE}_{\text{RBF}_{\text{update}}} - \text{MSE}_{\text{RBF18}}$  means that the  $\text{RBF}_{\text{update}}$  interpolator has a



**Fig. 7** The  $MSE_{RBF_{update}}$  based on MILES spectral library. The top-left panel displays the result in stellar atmospheric parameter space. The points mark the positions of test stars, and the grey level and point size characterize the test result MSE of the  $RBF_{update}$  interpolator. Here, MSE is the mean squared error between the interpolated and the original spectra of a test star. The top-right panel depicts the projection on the  $\lg T_{eff}$  and  $\lg g$  plane, the bottom-left panel displays the projection on the  $\lg g$  and  $[Fe/H]$  plane and the bottom right panel gives the projection on the  $\lg T_{eff}$  and  $[Fe/H]$  plane. The red “+” symbols and the corresponding letters express the positions of the stars for which their spectra are shown in Figure 8.

better performance, and the positive value means that the RBF18 interpolator has a better performance.

In Figure 9,  $MSE_{RBF_{update}} - MSE_{RBF18}$  is shown in the stellar atmospheric parameter space. The top-left panel gives the result in  $T_{eff}$ ,  $\lg g$  and  $[Fe/H]$  space. The other three panels list the corresponding three projections that are the same as those in Figure 7. The point size characterizes the absolute value of  $MSE_{RBF_{update}} - MSE_{RBF18}$ , the point color signifies the value  $MSE_{RBF_{update}} - MSE_{RBF18}$ . Here, blue and red points mean negative and positive values of  $MSE_{RBF_{update}} - MSE_{RBF18}$ , respectively.

On the whole, the test results of the  $RBF_{update}$  interpolator are better than those of the RBF18 interpolator. In the high temperature main sequence region, it does not have an obvious difference for the two interpolators. Panels

(a) and (b) in Figure 8 give two typical test results, and both two interpolators have smaller MSE. In the dense part of low-temperature main sequence and red giant regions, the  $RBF_{update}$  interpolator has better performance than the RBF18 interpolator with a lower MSE value. Two typical test spectra are shown in panels (c) and (d) in Figure 8, and the green interpolated spectra have a better match with the original spectra than the red ones.

However for some test stars on the edge of the low-temperature region, both  $RBF_{update}$  and RBF18 interpolators have bad performance. The spectra of four typical test stars in those regions are displayed in panels (e-h) of Figure 8, and a corresponding detailed analysis will be given in Section 4.3.

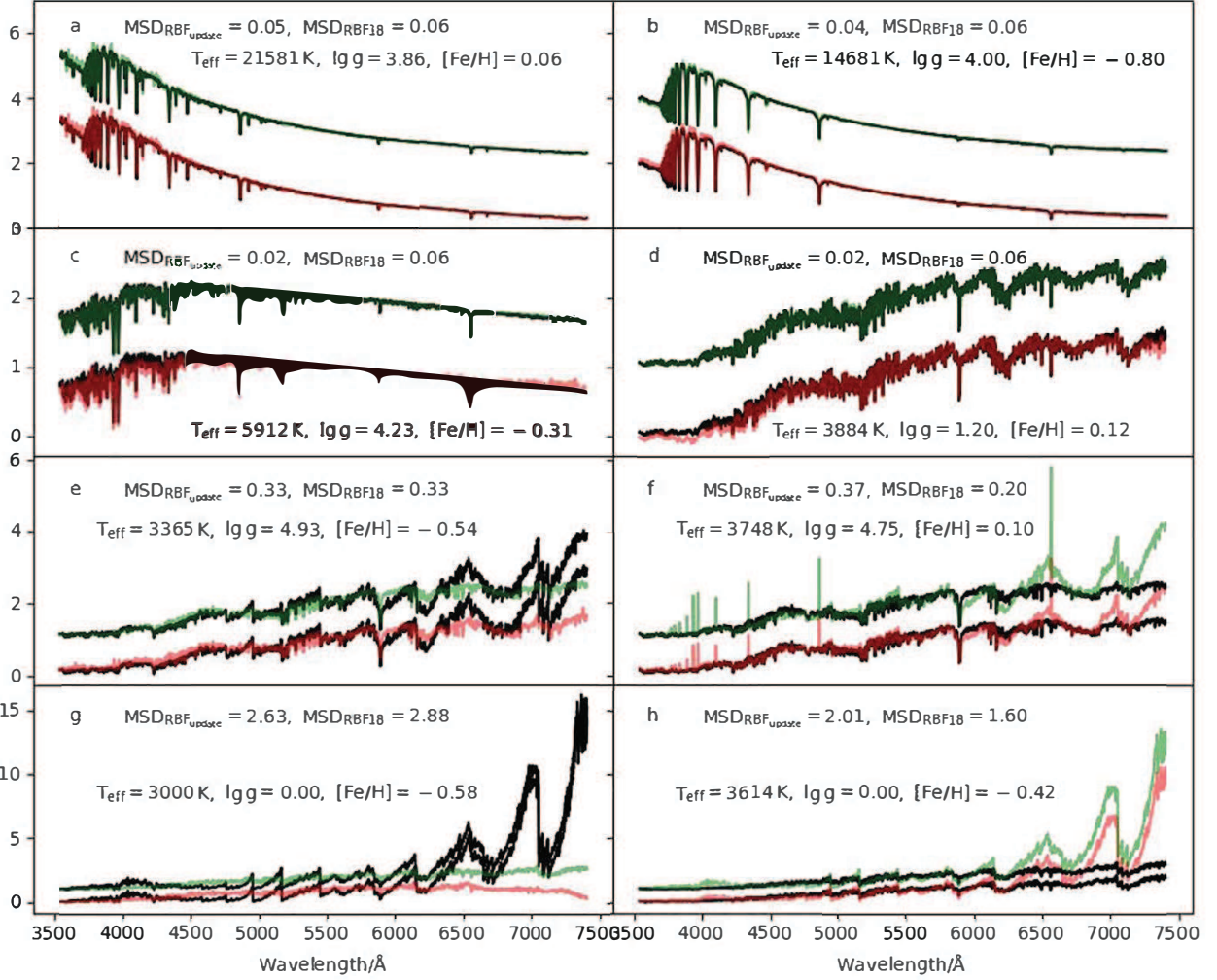


**Fig. 8** The spectra of eight test stars in the MILES library are signified by the red “+” symbols in Figure 7. The stellar atmospheric parameters and the test result MSE of RBF<sub>update</sub> and RBF18 interpolators also are listed. For every panel, three spectra are included. The black line is the original spectrum of test stars in the MILES library. The green and red translucent lines are the interpolated spectra of test stars by RBF<sub>update</sub> and RBF18 interpolators, respectively. For clarity, the interpolated spectra by the RBF<sub>update</sub> interpolator are shifted upwards, and the corresponding original spectrum also has a copy spectrum that is moved upwards by the same distance. Moreover, for avoiding overlap, the red and green lines are translucent. The first four panels (a-d) list four representative test spectra in different areas of stellar atmospheric space. Panels (e) and (f) express the representative bad interpolated spectra in the low-mass main sequence region. The last two panels, (g) and (h) provide the representative bad interpolated spectra in the red giant branch region.

### 4.3 Analysis of result

Here, we will give an analysis of the test result in Section 4.2. On the whole, the RBF<sub>update</sub> interpolator has better performance than the RBF18 interpolator in the spectral interpolation calculation. However, it has bad performance at the edge of the low-temperature region. A typical example of bad performance is displayed in the last four panels of Figure 8. Panels (e) and (f) show the test result of two test stars at the edge of the low-temperature main sequence region, and panels (g) and (h) depict the test result of two test stars at the edge of the red giant region. The positions of these four test stars are shown in Figure 7. We can find

the test stars in panels (e) and (f) are adjacent and those in panels (g) and (h) are adjacent. From the Gaussian kernel function (Eq. (3)), we know that the spectrum of the adjacent star has a bigger effect than the distant one in the interpolated calculation. Therefore, in the test, the calculation of the deleted spectrum depends largely on the adjacent spectra in the stellar atmospheric parameter space. For the test star in panel (e), star f has a big effect, which is the reason the interpolated spectrum in panel (e) is similar to the original spectrum in panel (f). For the interpolated spectra in panels (f), (g) and (h), the situations are similar.

For the empirical stellar spectral library, we list three possible reasons for the bad test results.

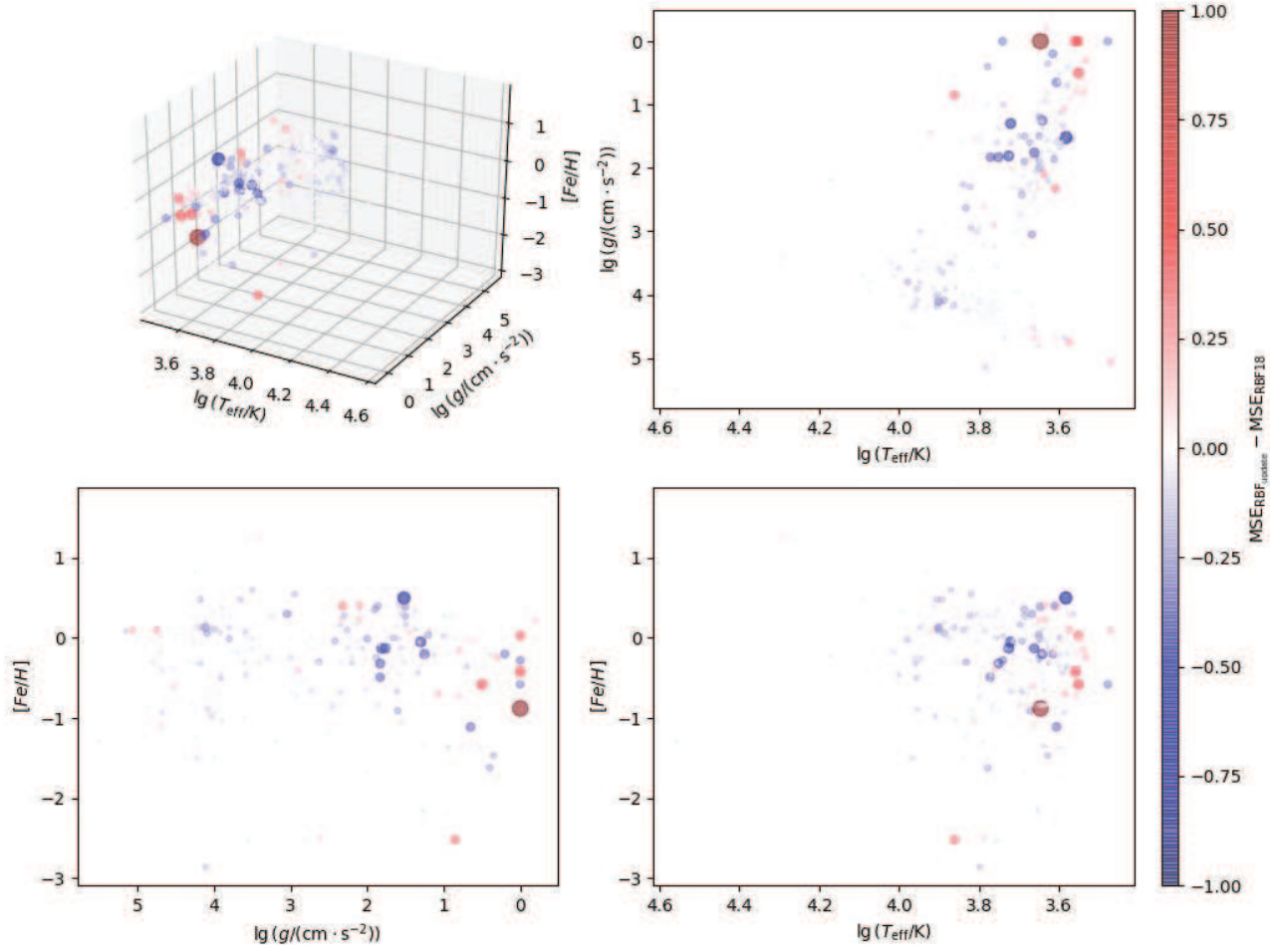


**Fig. 9** The discrepancy in the MSE between the  $\text{RBF}_{\text{update}}$  and  $\text{RBF}_{18}$  interpolators based on the MILES library. The points mark the positions of test stars. The color of points characterizes the value  $\text{MSE}_{\text{RBF}_{\text{update}}} - \text{MSE}_{\text{RBF}_{18}}$ , the blue points mean negative value and the red points mean positive value. The point size signifies the absolute value of  $\text{MSE}_{\text{RBF}_{\text{update}}} - \text{MSE}_{\text{RBF}_{18}}$ . The top-left panel displays the result in 3D stellar atmospheric parameters, the top-right panel gives the projection on the  $\lg T_{\text{eff}}$  and  $\lg g$  plane, the bottom-left panel displays the projection on the  $\lg g$  and  $[\text{Fe}/\text{H}]$  plane, and the bottom-right panel shows the projection on the  $\lg T_{\text{eff}}$  and  $[\text{Fe}/\text{H}]$  plane.

1. The finite spectra face a complex change in some stellar atmospheric parameter regions. It means that the library is incomplete and does not include enough typical spectra.
2. Three stellar atmospheric parameters cannot solely determine the spectra. It means that one set of stellar atmospheric parameters in 3D space corresponds to several potential spectra with obvious difference<sup>3</sup> (similar to the description in [Arentsen et al. 2019](#).)
3. The stellar atmospheric parameters are not self-consistent. The stellar spectra do not vary with the stellar atmospheric parameters by a one-to-one relation<sup>4</sup>.

<sup>3</sup> An example is that  $[\text{Fe}/\text{H}]$  cannot describe the ratio of the different elements in the stellar atmosphere. This problem does not have an obvious effect on the high-temperature region, but cannot be ignored in the low-temperature region.

<sup>4</sup> A simple example is that a smooth change of the spectra in the stellar atmospheric parameter space can be broken and becomes messy by

For the first reason, more targeted observational data are needed. For the second reason, more potential parameters of spectra should be given for a more strict constraint on the spectra. For the third reason, the spectra in the library need a more detailed derivation of atmospheric parameters, and we give a test by utilizing those self-consistent stellar atmospheric parameters. Here we consider a relatively new result of [Sharma et al. \(2016\)](#) to test this idea. In [Sharma et al. \(2016\)](#),  $\sim 300$  cool stars in the MILES library were refined. We replace the corresponding parameter of the MILES library by the results of [Sharma et al. \(2016\)](#), and use them to test  $\text{RBF}_{\text{update}}$  interpolator as did in Section 4.2.1. In Figure 10, we display the test results. The top panel shows the MSE distribution of test stars based on the MILES library with the original

adding a set of random biases in the stellar atmospheric parameters in the library.

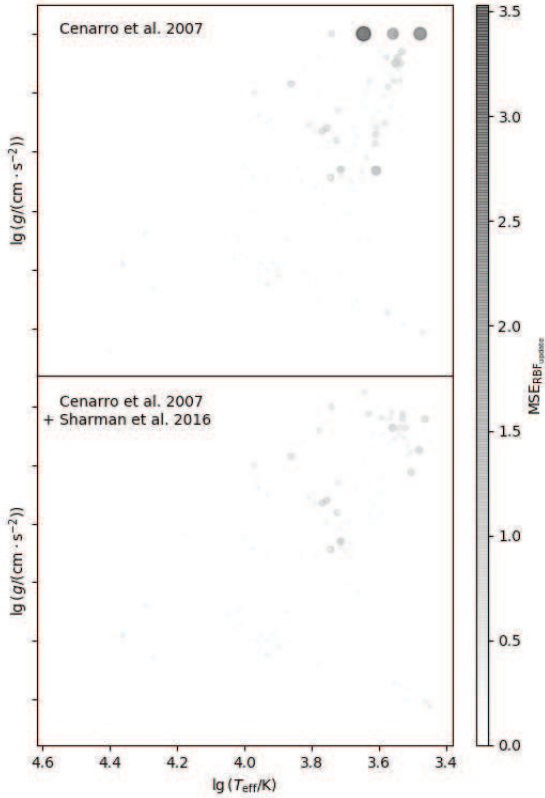


**Fig. 10** The MSE distribution of the test for the  $\text{RBF}_{\text{update}}$  interpolator on the  $\lg T_{\text{eff}}$  and  $\lg g$  plane. The top panel is the same as the top-right panel of Figure 7 and gives the resulting MSE distribution of the test which is based on the MILES library with its original stellar atmospheric parameters (Cenarro et al. 2007). In the bottom panel, we show the MSE distribution of the test based on the MILES library with the corrected cool stellar atmospheric parameters (Sharma et al. 2016). For every panel, the grey level and the size of points characterize the MSE values.

stellar atmospheric parameters (Cenarro et al. 2007). It is the same as the top-right panel in Figure 7, and the bottom panel features the MSE distribution of the test based on the MILES library with replaced stellar atmospheric parameters of the cool stars (Sharma et al. 2016). An obvious improvement appears in the bottom panel. This result demonstrates the self-consistent parameters of the library are important for the spectral interpolation calculation.

## 5 CONCLUSIONS

In stellar population synthesis models, the empirical stellar spectral library is necessary for the integrated spectra of the stellar populations. In this work, we improve the RBF network by comparing with the other kernel methods (SPHs and likelihood approximation) and give an upgraded spectral RBF interpolator. We include a constraint related to the kernel function (Eq. (7)) in the RBF network. This con-

straint expresses the relation between the  $\sigma$  of a Gaussian kernel function and the sample spatial density in the parameter space.

Moreover, we also consider the anisotropic kernel function by relating it to the inhomogeneous distribution of stars in the stellar atmospheric parameter space. We use the local axial direction dispersion to determine the anisotropic kernel function (Eq. (11)). By including three control parameters  $c_0, c_1, c_2$ , we can get an RBF network for spectral interpolation calculation. Here we call it an  $\text{RBF}_{\text{update}}$  interpolator. The BAS search algorithm is applied to search for the best control parameters  $c_0, c_1, c_2$  by matching with the semi-empirical BaSeL-3.1 stellar spectral library.

We also use a test to analyze the performance of the  $\text{RBF}_{\text{update}}$  interpolator based on the MILES stellar spectral library. In the test, we select any star in the MILES library as the test object and compare the original with the interpolated spectra which is calculated by the  $\text{RBF}_{\text{update}}$  interpolator based on the remaining stellar spectra in the MILES library. We find that the  $\text{RBF}_{\text{update}}$  interpolator has a good performance in general except for some test stars at the edge of the red giant and low-temperature main sequence regions (Fig. 7).

Three possible reasons can cause bad performance for empirical stellar spectral library. The first is the incomplete spectral coverage in the stellar atmospheric parameter space, the second is the existence of potential atmospheric parameters and the third is inconsistent atmospheric parameters. For the first two reasons, more observations are needed and additional atmospheric parameters should be included in the stellar spectral library. For the last reason, the modified stellar atmospheric parameters of the stellar spectral library are needed. Moreover, we also provide a comparison between the  $\text{RBF}_{\text{update}}$  interpolator and our early work in Cheng et al. (2018). The results show that the  $\text{RBF}_{\text{update}}$  interpolator has an obvious improvement, except for the edge of the low-temperature region (Fig. 9). The same reasons make both interpolators not have a good performance in these regions.

At last, the code of  $\text{RBF}_{\text{update}}$  interpolator is written in Python and you can find it at <http://www1.yao.ac.cn/~zhangfh/>. The code can be implemented for different libraries and a user can apply it with the modified stellar spectral library by adding additional spectra or updating the stellar atmospheric parameters of the library.

**Acknowledgements** This project was partly supported by the Chinese Natural Science Foundation (grants 11973081, 11573062 and 11521303), Youth Innovation Promotion Association (grant 2012048) and the Yunnan Foundation (grant 2011CI053).

**References**

- Arentsen, A., Prugniel, P., Gonneau, A., et al. 2019, *A&A*, 627, A138
- Bicknell, G. V., & Gingold, R. A. 1983, *ApJ*, 273, 749
- Broomhead, D. S., & Lowe, D. 1988, *Complex Systems*, 2, 321
- Bruzual, G., & Charlot, S. 2003, *MNRAS*, 344, 1000
- Cenarro, A. J., Peletier, R. F., Sánchez-Blázquez, P., et al. 2007, *MNRAS*, 374, 664
- Chen, Y.-P., Trager, S. C., Peletier, R. F., et al. 2014, *A&A*, 565, A117
- Cheng, L., Zhang, F., Kang, X., & Wang, L. 2018, *MNRAS*, 476, 4071
- Choi, J., Dotter, A., Conroy, C., et al. 2016, *ApJ*, 823, 102
- Ding, C. H. Q., & He, X. 2004, in *ACM International Conference Proceeding Series*, Vol. 69, *Machine Learning, Proceedings of the Twenty-first International Conference (ICML 2004)*, Banff, Alberta, Canada, July 4-8, 2004, ed. C. E. Brodley (ACM)
- Dotter, A. 2016, *ApJS*, 222, 8
- González Delgado, R. M., Cerviño, M., Martins, L. P., Leitherer, C., & Hauschildt, P. H. 2005, *MNRAS*, 357, 945
- Jiang, X., & Li, S. 2017, arXiv:1710.10724
- Kurucz, R. L. 1992, in *IAU Symposium*, Vol. 149, *The Stellar Populations of Galaxies*, ed. B. Barbuy & A. Renzini, 225
- Kurucz, R. L. 2014, *Problems with Atomic and Molecular Data: Including All the Lines, Determination of Atmospheric Parameters of B*, 63
- Le Borgne, J. F., Bruzual, G., Pelló, R., et al. 2003, *A&A*, 402, 433
- Lejeune, T., Cuisinier, F., & Buser, R. 1997, *A&AS*, 125, 229
- Lejeune, T., Cuisinier, F., & Buser, R. 1998, *A&AS*, 130, 65
- Lowe, D. 1989, in 1989 First IEE International Conference on Artificial Neural Networks, (Conf. Publ. No. 313), 171
- MacQueen, J. 1967, Some methods for classification and analysis of multivariate observations., *Proc. 5th Berkeley Symp. Math. Stat. Probab.*, Univ. Calif. 1965/66, 1, 281-297 (1967).
- Micchelli, C. A. 1986, *Constructive Approximation*, 2, 11
- Mollá, M., García-Vargas, M. L., & Bressan, A. 2009, *MNRAS*, 398, 451
- Owen, J. M., Villumsen, J. V., Shapiro, P. R., & Martel, H. 1998, *ApJS*, 116, 155
- Paxton, B., Bildsten, L., Dotter, A., et al. 2011, *ApJS*, 192, 3
- Paxton, B., Cantiello, M., Arras, P., et al. 2013, *ApJS*, 208, 4
- Paxton, B., Marchant, P., Schwab, J., et al. 2015, *ApJS*, 220, 15
- Paxton, B., Schwab, J., Bauer, E. B., et al. 2018, *ApJS*, 234, 34
- Powell, M. J. D. 1987, *Radial Basis Functions for Multivariable Interpolation: A Review, Algorithms for Approximation (USA: Clarendon Press)*, 143
- Prugniel, P., & Soubiran, C. 2001, *A&A*, 369, 1048
- Prugniel, P., Vauglin, I., & Koleva, M. 2011, *A&A*, 531, A165
- Sánchez-Blázquez, P., Peletier, R. F., Jiménez-Vicente, J., et al. 2006, *MNRAS*, 371, 703
- Shapiro, P. R., Martel, H., Villumsen, J. V., & Owen, J. M. 1996, *ApJS*, 103, 269
- Sharma, K., Prugniel, P., & Singh, H. P. 2016, *A&A*, 585, A64
- Westera, P., Samland, M., Bruzual, G., & Buser, R. 2002, *Astronomical Society of the Pacific Conference Series*, Vol. 274, *The BaSeL 3.1 models: metallicity calibration and application*, ed. T. Lejeune & J. Fernandes, 166
- Wu, Y., Luo, A. L., Li, H.-N., et al. 2011, *RAA (Research in Astronomy and Astrophysics)*, 11, 924
- Zhang, F., Li, L., Han, Z., Zhuang, Y., & Kang, X. 2013, *MNRAS*, 428, 3390